Anal. Chem. **2007,** *79,* 9261−9268

Measurement of Sulfur Isotope Compositions by Tunable Laser Spectroscopy of SO_2

Lance E. Christensen,* Benjamin Brunner,† Kasey N. Truong, Randall E. Mielke, Christopher R. Webster, and Max Coleman

Jet Propulsion Laboratory, California Institute of Technology, Pasadena, California, 91109

Sulfur isotope measurements offer comprehensive information on the origin and history of natural materials. Tunable laser spectroscopy is a powerful analytical technique for isotope analysis that has proven itself readily adaptable for in situ terrestrial and planetary measurements. Measurements of $\delta^{34}S$ in SO_2 were made using tunable laser spectroscopy of combusted gas samples from six sulfur-bearing solids with $\delta^{34}S$ ranging from −34 to +22‰ (also measured with mass spectrometry). Standard deviation between laser and mass spectrometer measurements was 3.7‰ for sample sizes of 200 ± 75 nmol SO_2. Although SO_2(g) decreased 9% over 15 min upon entrainment in the analysis cell from wall uptake, observed fractionation was insignificant (+0.2 ± 0.6‰). We also describe a strong, distinct $^{33}SO_2$ rovibrational transition in the same spectral region, which may enable simultaneous $\delta^{34}S$ and $\Delta^{33}S$ measurements.

Sulfur isotope analysis has a wide range of applicability including sourcing atmospheric sulfur pollution,[1] chronicling the emergence of life,[2] and determining when atmospheric oxygen became abundant.[3] Sulfur isotope measurements have great potential for furthering planetary science by characterizing the origin and history of sulfate deposits on Mars[4] and by providing evidence of past or extant life on Europa.[5] For these reasons, there are many benefits in developing field instrumentation for in situ sulfur isotope analysis.

Semiconductor laser spectroscopy is a well-established analytical technique for high-sensitivity detection of trace gas-phase species.[6] Continuing advancement of thermoelectrically cooled, single-mode, mid-infrared emitting type III−V, quantum-cascade, and interband-cascade semiconductor lasers, has resulted in complementary advancement of compact, high-accuracy semiconductor laser spectrometers.

Application of laser spectroscopy to isotopic analysis is recent in comparison to isotope ratio mass spectrometry (IRMS). IRMS is the original and prevalent method for making measurements of variations in stable isotope ratios[7] and produces precise results in the laboratory, on the order of 0.02‰ on sample sizes as small as 1 μmol. Laser spectroscopy has not yet achieved such precision for isotopic analysis, but substantial progress has been made within the past 5 years. Spectrometers utilizing semiconductor lasers have demonstrated measurement sensitivites between 0.1 and 0.5‰ for $\delta^{13}C$ in CO_2,[8,9] and between 0.2 and 0.5‰ for $\delta^{18}O$, $\delta^{17}O$, and δD in H_2O.[10] Currently, there are no published accounts of the application of laser spectroscopy to isotopic analysis of sulfur dioxide.

Laser spectroscopy is an attractive alternative to IRMS for isotope analysis for several reasons. Laser spectrometers can discern distinct isotopomers of nearly identical mass since isotopomers have unique spectral fingerprints. In the case of sulfur isotopes, sulfur is typically converted to SO_2(g) for analysis. However, interference between $^{34}SO_2$ and $SO^{18}O$ must be corrected in IRMS.[11] There is also mass overlap between $^{33}SO_2$ and $SO^{17}O$. To circumvent this problem, sulfur can be converted to SF_6, but the difficulty in chemical conversion hinders miniaturization. Another advantage of laser spectroscopy is that, for field work, laser spectrometers are generally more compact and lightweight than their mass spectrometer counterparts. An example of this is underscored by the recent selection of the tunable laser spectrometer (TLS)[12] for measuring isotope ratios in CO_2 and CH_4 as part of the Sample Analysis at Mars (SAM) suite on the 2009 Mars Science Lab (MSL) mission. Concurrent miniaturization of IRMS instrumentation is also an ongoing endeavor—SAM will also utilize a compact, quadrupole mass spectrometer that will, in addition to other measurements, analyze sulfur isotope ratios at precisions between 5 and 10‰.[13] Also, there has been considerable progress in the miniaturization of ion-trap mass spectrometers in recent years.[14]

* To whom correspondence should be addressed. E-mail: Lance.E.Christensen@jpl.nasa.gov. Fax 818-354-4445.

† Current address: Max Planck Institute for Marine Biology, D-28359 Bremen, Germany.

(1) Nriagu, J. O.; Coker, R. D.; Barrie, L. A. *Nature* **1991**, *349*, 142−145.
(2) Shen, Y.; Buick, R.; Canfield, D. E. *Nature* **2001**, *410*, 77−81.
(3) Farquhar, J.; Bao, H.; Thiemens, M. *Science* **2000**, *289*, 756−758.
(4) Farquhar, J.; Savarino, J.; Jackson, T. L.; Thiemens, M. H. *Nature* **2000**, *404*, 50−52.
(5) Chela-Flores, J. *Int. J. Astrobiol.* **2006**, *5*, 17−22.
(6) Werle, P. *Spectrochim. Acta, A* **1998**, *54*, 197−236.
(7) McKinney, C. R.; McCrea, J. M.; Epstein, S.; Allen, H. A.; Urey, H. C. *Rev. Sci. Instrum.* **1950**, *21*, 724−730.
(8) Castrillo, A.; Casa, G.; Kerstel, E.; Gianfrani, L. *Appl. Phys. B* **2005**, *81*, 863−869.
(9) McManus, J. B.; Nelson, D. D.; Shorter, J. H.; Jimenez, R.; Herndon, S.; Saleska, S.; Zahniser, M. *J. Mod. Opt.* **2005**, *52*, 2309−2321.
(10) Gianfrani, L.; Gagliardi, G.; van Burgel, M.; Kerstel, E. R. T. *Opt. Express* **2003**, *11*, 1566−1576.
(11) Coleman, M. L. In *Handbook of Stable Isotope Analytical Techniques*; de Groot, P. A., Ed.; Elsevier: Amsterdam, ,The Netherlands, 2004; pp 957−970.
(12) Atreya, S.; Mahaffy, P. R.; Wong, A.-S. *Planet. Space Sci.* **2007**, *55*, 358−369.
(13) Mahaffy, P. Personal communication, 2007.
(14) Blain, M. G.; Riter, L. S.; Cruz, D.; Austin, D. E.; Wu, G.; Plass, W. R.; Cooks, R. G. *Int. J. Mass Spectrom.* **2004**, *236*, 91−104.

10.1021/ac071040p CCC: $37.00
Published on Web 11/17/2007

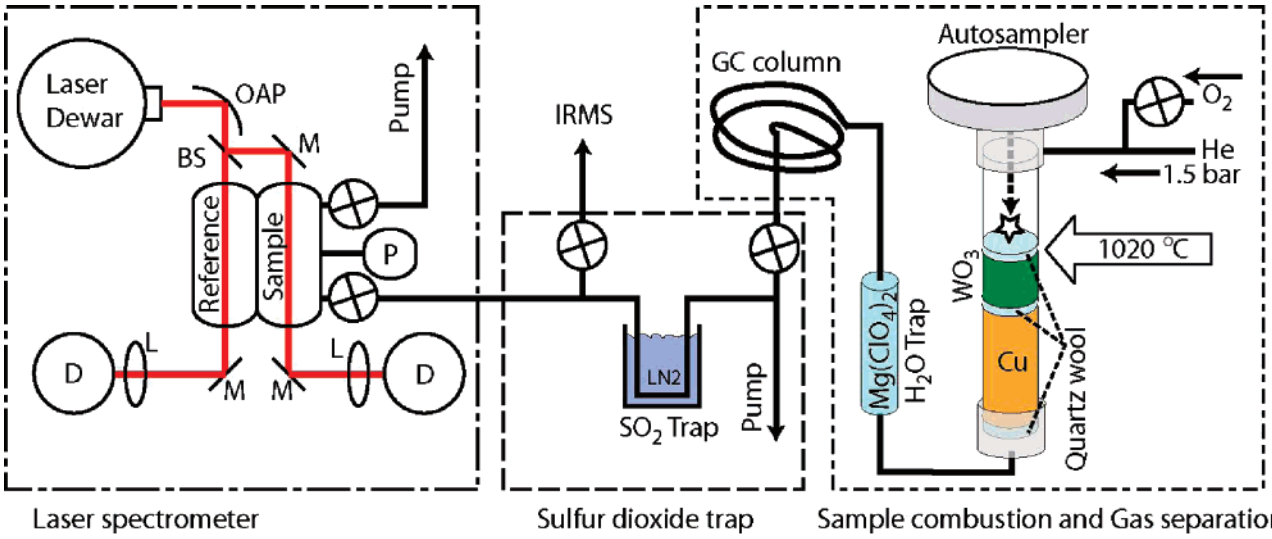

Figure 1. Schematic of laboratory setup. Components: flat mirrors (M), off-axis parabolic mirrors (OAP), positive-meniscus lens (L), pressure transducer (P), MCT detectors (D), pellicle beam splitter (BS), valves (⊗). Red line represents the laser beam.

A number of comprehensive reviews describe ranges of naturally occurring and anthropogenically affected sulfur isotope values.[15,16] The most significant terrestrial fractionation process involves sulfate-reducing bacteria, which produce isotopically light (negative $\delta^{34}S$) sulfide, and it is these processes that account for the large range of values exhibited in sedimentary rocks. Dissolved sulfide tends to precipitate out of aqueous solution, and the remaining sulfate reservoir becomes enriched in ^{34}S. Values of $\delta^{34}S$ in sulfur-bearing rocks have been observed to be as low as −65‰ in sulfides and as high as +120‰ in sulfates.[17] Sulfur isotope ratios can be interpreted to indicate details of past geological processes in sediments[18] and give quantitative estimates of temperature of formation and mode of genesis of sulfide ores. On Mars, sulfates have been extensively observed, though their isotopic compositions are unknown. Measurements of the $\delta^{34}S$ of these sulfates would help determine their origin and confirm or contradict conflicting theories about past amounts of liquid water on Mars and its ability to support life.[19]

Thus, there are many applications where in situ field measurements of sulfur isotope compositions would be of significant value. Semiconductor laser spectroscopy offers a possibility for making sensitive analyses to meet these needs.

EXPERIMENTAL SECTION

The experimental setup is depicted in Figure 1. Six materials were analyzed. Four were different barium sulfates: IAEA-SO-5, IAEA-SO-6, NBS-127, and $BaSO_4$-lab. The other two were silver sulfides: NZ-2 and strontium sulfate, $SrSO_4$-lab. Materials IAEA-SO-5, IAEA-SO-6, NBS-127, and NZ-2 are international standards while $BaSO_4$-lab and $SrSO_4$-lab are internal laboratory standards whose values are determined by comparing with international standards.

The conventional expression of isotopic ratio is as a difference between sample and reference in parts per thousand (‰), normalized to the reference ratio:

$$\delta^{34}S = 1000[(^{34}S/^{32}S)_{sample} - (^{34}S/^{32}S)_{VCDT}]/(^{34}S/^{32}S)_{VCDT} \quad (1)$$

The International Atomic Energy Agency (IAEA) and the International Union of Pure and Applied Chemistry (IUPAC) established the Vienna Cañon Diablo Troilite (VCDT) scale, in which IAEA-S-1 is defined as $\delta^{34}S = -0.3$‰ exactly.[20] The four naturally occurring isotopes of sulfur are nonradioactive with abundances: ^{32}S (94.93%), ^{33}S (0.76%), ^{34}S (4.29%), and ^{36}S (0.02%).[21]

IRMS Measurements and Sample Preparation. Two sets of IRMS measurements were conducted. The first set established $\delta^{34}S$ of the lab-standard materials prior to laser analysis and involved no cryogenic trapping. The second set, conducted during laser analysis, was derived from aliquots of the same solid samples analyzed in the first set and provided a correction factor for effects of cryogenic SO_2 trapping.

In both cases, continuous flow IRMS was performed on SO_2 produced online from combusted powdered solid samples. Sample weight was 600−800 μg for $BaSO_4$, 200−300 μg for silver sulfide, and 500−600 μg for strontium sulfate, corresponding to 2.3−3.5 μmol SO_2 produced. Samples were weighed into tin capsules to which 500−800 μg vanadium pentoxide was added to aid oxidation. The capsules were tightly folded and placed into a helium-purged autosampler (Zero-Blank Autosampler, Costech Analytical Technologies Inc., Valencia, CA). Samples were dropped into a combustion tube at 1020 °C, and introduction of a pulse of

(15) Coplen, T. B.; Bohlke, J. K.; De Biévre, P.; Ding, T.; Holden, N. E.; Hopple, J. A.; Krouse, H. R.; Lamberty, A.; Peiser, H. S.; Revesz, K.; Rieder, S. E.; Rosman, K. J. R.; Roth, E.; Taylor, P. D. P.; Vocke, J., R. D.; Xiao, Y. K. *Pure Appl. Chem.* **2002**, *74*, 1987−2017.
(16) Krouse, H. R., Coplen, T. B.. Eds. Reporting of relative sulfur isotope-ratio data, International Union of Purer and Applied Chemistry (IUPAC); *Pure Appl. Chem.* **1997**, *69*.
(17) Hoefs, J. *Stable Isotope Geochemistry*, 5 ed.; Springer: Berlin, 2004.
(18) Coleman, M. L.; Raiswell, R. *Am. J. Sci.* **1995**, *295*, 282−308.
(19) McCollom, T. M.; Hynek, B. M. *Nature* **2005**, *438*, 1129−1131.
(20) Coplen, T. B.; Krouse, H. R. *Nature* **1998**, *392*, 32.
(21) Rosman, K. J. R.; Taylor, P. D. P.; International Union of Pure and Applied Chemistry (IUPAC), 1997.

Table 1. Samples and Results

label	material	MS, ‰	laser, ‰	N
A	$BaSO_4$ (lab-standard)	16.00	17.5	3
B	$BaSO_4$ (NBS-127)	20.30	22.8	2
C	Ag_2S (NZ-1)	−0.30	7.0	2
D	$BaSO_4$ (IAEA-SO-6)	−34.20	−34.8	2
E[a]	$BaSO_4$ (IAEA-SO-5)	0.48	0.48	3
F	$SrSO_4$ (lab-standard)	22.00	22.8	3

[a] This material was used for laser reference values.

O_2 induced exothermic combustion. Under these conditions, in the presence of a vanadium pentoxide and tungstic oxide tube packing, sulfur from the samples was converted into SO_2 and SO_3. Helium carrier gas transported these evolved gases downstream in the reaction tube where a copper packing reduced SO_3 to SO_2, leading to a SO_2 yield corresponding to quantitative conversion of sample sulfur to SO_2. The gas was dehydrated by passing through a trap packed with $Mg(ClO_4)_2$, and the SO_2 was isolated from other gases by a gas chromatography column.

The first set of IRMS measurements confirmed our ability to measure international standards correctly and gave calibrated values for laboratory standards listed in Table 1. Reproducibility was better than ±0.2‰ (1σ), demonstrating that preparation of SO_2 gas from solid samples yields highly reproducible sulfur isotope compositions.

For the second set of IRMS measurements, a liquid nitrogen-cooled cryogenic trap (LN2 trap) was added to capture SO_2. During SO_2 trapping, the flow of the helium carrier gas was directed to the IRMS. This allowed monitoring and analysis of the sulfur isotope composition of SO_2 that escaped trapping. The amount of SO_2 not captured was ~1.5% with enrichment in ^{34}S of 8 ± 2‰. Consequently, by mass balance, trapped gas was depleted in ^{34}S by −0.12 ± 0.08‰.

After SO_2 was trapped, the trap was evacuated to 1 mbar. This procedure was kept as short as possible, 30 ± 5 s, to avoid sublimation of SO_2, which would result in sample loss and isotope fractionation. Subsequently, LN2 was removed and the trap heated with a hot air gun. The SO_2 and remaining He expanded into the laser spectrometer. When sufficient sample gas was entrained in the laser spectrometer, the valve to the laser spectrometer was closed and measurements were taken. The mole fraction of SO_2 in the entrained gas was ~0.6, the balance being helium, with concentration (0.5−1.2) × 10^{16} molecules cm^{-3}, equal to 115−280 nmol of SO_2.

Laser Spectrometer. Laser dewar, optics, analysis cell, and detectors were enclosed in an acrylic glass box (55 cm × 55 cm × 39 cm) with gas and electric feed-throughs. Sample and reference cells were contained within the same aluminum block (17 cm × 5 cm × 9 cm) and separated by 0.5 cm. The reference cell contained SO_2 gas (Matheson Inc., anhydrous 99.98%, $^{34}S/^{32}S \approx 0.04$). Temperature was measured with a thermistor located between them. Experiments were conducted over 23.5−24.2 °C. Total pressure of the gas samples ranged from 0.6 to 1.6 mbar, determined by a Digiquartz 6015A pressure transducer (Paroscientific Inc., Redmond, WA).

A poly(tetrafluoroethylene) (PTFE) insert was fixed inside the aluminum sample cell, which served to reduce the volume into which the sample gas was entrained, thereby increasing SO_2 concentration and its absorption signal. Total internal volume was 14 cm^3 including conduits to the valves with surface area of 56 cm^2, consisting mainly of PTFE (~90%), CaF_2 windows, and 316 stainless steel.

Sample and reference gas were probed via emission at 7.4 μm from a lead-salt diode laser (Laser Components IG Inc.) housed in a liquid nitrogen-cooled dewar (OLS150/2, Mütek Infrared Laser Systems, Diessen, Germany). The diode laser temperature was controlled by a commercial temperature controller (TLS150, Mütek). The laser beam was split into two parts by a pellicle beam splitter. One part made a single pass (16.5-cm optical path length) through the sample cell, and the other made a single pass (16.5-cm optical path length) through the reference cell, impinging on separate LN2-cooled HgCdTe detectors (InfraRed Associates, Inc., Stuart, FL). A low-frequency (20 Hz) sawtooth laser current ramp was applied to the laser, which tuned the emission frequency over several SO_2 rovibrational transitions. Both direct absorption spectroscopy and second-harmonic wavelength-modulation spectroscopy (WMS) were applied.[22] For WMS measurements, high-frequency (20 kHz) sinusoidal laser current modulation was imposed on the low-frequency ramp. The high-frequency modulation was turned on and off during successive scans resulting in collection of interlaced direct absorption and WMS signals. Ten successive scans were averaged and written to disk every 1.6 s, with additional time needed for pressure and temperature measurement and processing overhead.

Measurements presented here were derived only from the sample cell. The reference cell was used to qualitatively monitor for large-scale temperature changes and changes in laser performance. Initially, we planned to utilize reference cell measurements to remove noise common to sample and reference channels. However, we found this procedure did little to improve our results. Also, there was a systematic offset, greater than 0.2%, in ratio measurements between sample and reference channels when probing the same gas. This may be due to differences in detector responsivity and associated electronics preceding digitization of the separate signals.

Measurements were taken over 12 h on six materials listed in Table 1. Three consecutive samples of each material were measured. Of 18 measurements, 3 are not included in the final analysis due to complications in gas entrainment and data acquisition. Each laser spectrometer measurement lasted 15 min. During intervals between each measurement, the foreline and laser spectrometer sample cell were pumped continuously between 7 and 11 min.

SPECTROSCOPY

Sulfur dioxide is an asymmetric rotor with three fundamental vibrational modes, all IR-active. The spectral region near 7.4 μm was probed because it contains transitions belonging to the strongest absorption band, 001-000 (asymmetric stretch). The band centers for 001-000 of $^{32}SO_2$ and $^{34}SO_2$ are 1362 and 1345 cm^{-1}, respectively. Transitions originating from the 011-010 hot band of $^{32}SO_2$ must be taken into account since the vibrationally excited state is significantly populated, ~8%, at 298 K.

(22) Moses, E. G.; Tang, C. L. *Opt. Lett.* **1977**, *1*, 115−117.

The HITRAN 2004[23] and GEISA-03[24] spectral databases contain information only on 001-000 of $^{32}SO_2$. However, parameters for 001-000 of $^{34}SO_2$ and 011-010 of $^{32}SO_2$ exist in the literature. The 001-000 band of $^{34}SO_2$ was modeled using the parameters given in Guelachvili et al.[25] For 011-010 of $^{32}SO_2$, transitions were modeled using 011 from Guelachvili et al.[25] and 010 from Flaud et al.[26] Modeling was done with the SPCAT rovibrational transition prediction program.[27] Deviating from the procedure adopted for HITRAN, line strengths for 001-000 of $^{32}SO_2$ were scaled by 1.0574 to remove prior isotopic abundance scaling, the values of 001-000 of $^{34}SO_2$ were left unscaled, and those of the 011-010 band for $^{32}SO_2$ were scaled to the 001-000 band by 0.089 to account for the difference in ground-state energy. Experimental and modeling work by Chu et al. concluded that HITRAN 2004 line strengths for 000-001 are too high by 10−25%.[28]

To increase confidence in modeling results and to find a suitable pair of $^{32}SO_2$ and $^{34}SO_2$ features useful for isotopic ratio measurements, separate experiments on two different SO_2 gas samples were performed. One contained $^{34}S/^{32}S \approx 0.04$ (Matheson Inc., anhydrous 99.98%), and the other contained $^{34}S/^{32}S \approx 90$ (Icon Services Inc., Summit, NJ). The laser frequency was scanned over several spectral regions between 1344.7 and 1359.6 cm^{-1}. One region is provided in Supporting Information Figure S-1. Water lines and a solid germanium etalon were used determine frequency. Additional checks using the JPL MkIV Fourier transform infrared (FT-IR) spectrometer[29] were also done. Measured features could be confidently assigned for $J < 18$, which permitted calculation of ground-state energy (for temperature dependence) and line strength (for concentration). Uncertainty in line strength is estimated to be 20% considering potential errors from phenomena not included in modeling such as resonance effects and Herman-Wallis intensity factors.

After modeling and experimental verification of the spectroscopy of $^{32}SO_2$ and $^{34}SO_2$, we were in a position to select an appropriate spectral window for isotopic ratio measurements.

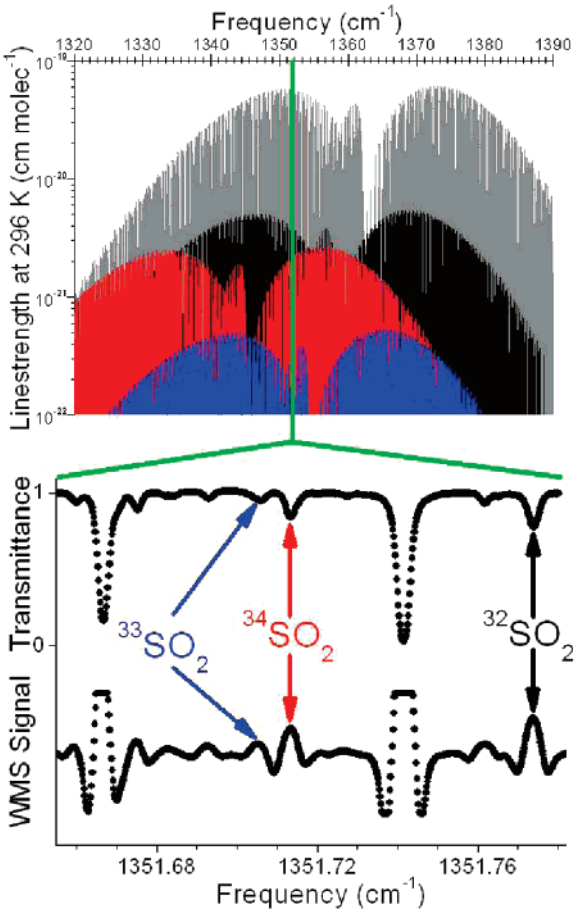

Figure 2. Top: Modeled band diagram for 001-000 of $^{32}SO_2$ (gray), 011-010 of $^{32}SO_2$ (black), 001-000 of $^{34}SO_2$ (red), and 001-000 of $^{33}SO_2$ (blue). Bottom: Experimental spectra of a combusted sample of $BaSO_4$ (IAEA-SO-6). $^{34}SO_2$ and $^{32}SO_2$ features denoted in the figure were used to measure $\delta^{34}S$. Data in the flat portions of the WMS signal for the two strongest absorption features were off-scale for the digitizer. Also denoted is a $^{33}SO_2$ transition.

RESULTS

Measured Spectra. We conducted isotopic ratio measurements between 1351.65 and 1351.80 cm^{-1}. Simultaneous direct absorption and WMS spectra of a combusted sample of $BaSO_4$ IAEA-SO-6 are shown in Figure 2. This spectral window was selected because it contains a strong $^{34}SO_2$ transition in proximity to $^{32}SO_2$ transitions of similar line strength in a region free of water interference. It is also a region in which the diode laser light emission was greater than 99% single mode as ascertained via spectra provided by the laser manufacturer and verified in our laboratory by performing saturated absorption measurements. Modeled parameters for transitions in this region are given in Supporting Information Table S-1. Separate FT-IR analysis of $^{33}SO_2$ gas samples (Icon Services Inc.) indicated that $^{33}SO_2$ lines in this spectral window did not interfere with measurements of $\delta^{34}S$.

The two features chosen for $\delta^{34}S$ measurements are denoted in Figure 2. The feature at 1351.713 cm^{-1} is $^{34}SO_2$ and the one at 1351.774 cm^{-1} belongs to two overlapped $^{32}SO_2$ transitions. The WMS signal is the integrated, second-order Fourier component of the direct absorption signal, and its value depends on the direct absorption profile and applied current modulation amplitude.[6] Strategies and details for measuring isotope ratios via laser spectroscopy are found in a comprehensive review.[30]

Here, three measurements of each isotopomer x were made: W_x, the difference between the peak and one of the negative lobes of the WMS signal; P_x, the power at line center with SO_2 present; $P_{0,x}$, the power at line center with SO_2 absent, interpolated from the background signal. P_x and $P_{0,x}$ were derived from the direct absorption spectrum. The high-frequency negative lobe (1351.717

(23) Rothman, L. S.; Jacquemart, D.; Barbe, A.; Benner, D. C.; Birk, M.; Brown, L. R.; Carleer, M. R.; Chackerian, C., Jr.; Chance, K.; Coudert, L. H.; Dana, V.; Devi, V. M.; Flaud, J. M.; Gamache, R. R.; Goldman, A.; Hartman, J. M.; Jucks, K. W.; Maki, A. G.; Mandin, J. Y.; Massie, S. T.; Orphal, J.; Perrin, A.; Rinsland, C. P.; Smith, M. A. H.; Tennyson, J.; Tolchenov, R. N.; Toth, R. A.; Vander Auwera, J.; Varanasi, P.; Wagner, G. *J. Quant. Spectrosc. Radiat. Transfer* **2005**, *96*, 139−204.

(24) http://ara.lmd.polytechnique.fr/htdocs-public/products/GEISA/HTML-GEISA/GeisaLine.html.

(25) Guelachvili, G.; Naumenko, O. V.; Ulenikov, O. N. *J. Mol. Spectrosc.* **1987**, *125*, 128−139.

(26) Flaud, J.-M.; Perrin, A.; Salah, L. M.; Lafferty, W. J.; Guelachvili, G. *J. Mol. Spectrosc.* **1993**, *160*, 272−278.

(27) Pickett, H. *J. Mol. Spectrosc.* **1991**, *148*, 371−377.

(28) Chu, P. M.; Wetzel, S. J.; Lafferty, W. J.; Perrin, A.; Flaud, J. M.; Arcas, P.; Guelachvili, G. *J. Mol. Spectrosc.* **1998**, *189*, 55−63.

(29) Toon, G. C. *Opt. Photonics News* **1991**, *2*, 19−21.

(30) Kerstel, E. In *Handbook of Stable Isotope Analytical Techniques*; de Groot, P. A., Ed.; Elsevier: Amsterdam, The Netherlands, 2004; Vol. 1.

cm^{-1}) was used for W_{34} and the low-frequency negative lobe (1351.770 cm^{-1}) was used for W_{32}.

From P_x and $P_{o,x}$, fractional absorption, α_x, was determined from the Beer−Lambert law

$$\alpha_x \equiv 1 - P_x/P_{o,x} = 1 - \exp(-\sigma_x \cdot l \cdot [x]) \quad (2)$$

where $[x]$ is SO_2 concentration, σ_x is the cross section at line center, and l is optical path length. Though σ_x, and hence α_x, are functions of light frequency, the present work focuses on their values at line center.

We utilized W_x for isotopic measurements because WMS achieves a significantly better signal-to-noise ratio than direct absorption spectroscopy.[31] To do so, the relationship between W_x and α_x needed to be established. W_x depends on the direct absorption line shape, which in turn, depends on fractional absorption, pressure, and temperature. The line shape is significantly affected by the nonlinearity of light absorption expressed in eq 2. As α_x increases, the absorption profile flattens. Since each isotopomer in the present experiment has a different fractional absorption, the flattened absorption profile will affect W_{34}/W_{32}. To correct for this, a scaling factor, Γ_x, was calculated so that $W_x\Gamma_x$ was proportional to α_x. Specifically,

$$W_x\Gamma_x = \gamma P_{o,x}\alpha_x \quad (3)$$

where γ is a constant that is a function of current modulation amplitude and incorporates electronics gain. More precisely, γ is slightly different for each isotopomer but, for simplicity, was assumed the same for each isotopomer with negligible effect on final results. The dependence of Γ_x on α_x was numerically modeled and is described in detail in Supporting Information Figure S-2. Γ_x was found to be

$$\Gamma_x = 1.0000 + 0.09062\alpha_x + 0.12029\alpha_x^2 \quad (4)$$

In the limit of zero fractional absorption, Γ_x approaches 1. If fractional absorption is equivalent for each isotopomer, Γ_x can be ignored when taking the ratio of signals. Here, $\langle\alpha_{34}\rangle = 0.18$ and $\langle\alpha_{32}\rangle = 0.13$, giving $\Gamma_{34}/\Gamma_{32} = 1.0063$. We modeled pressure and temperature effects on W_{34}/W_{32} through changes in the line shape broadening and found their effects negligible.

Using eq 2 and employing the Taylor series expansion for $\ln(1 - \alpha_x)$, isotopic ratios were analyzed as

$$^{34}S/^{32}S = (\sigma_{32}/\sigma_{34})(\alpha_{34}/\alpha_{32})(\Phi_{34}/\Phi_{32}) \quad (5)$$

$$\Phi_x = \sum_{n=0}^{\infty} \frac{\alpha_x^n}{n+1} \quad (6)$$

where $^{34}S/^{32}S$ denotes $[^{34}SO_2]/[^{32}SO_2]$. For typical fractional absorptions, $\Phi_{34}/\Phi_{32} = 0.971$. Combining eqs 3 and 5, the expression for $^{34}S/^{32}S$ is

$$^{34}S/^{32}S = (W_{34}/W_{32})(P_{o,32}/P_{o,34})(\sigma_{32}/\sigma_{34})(\Phi_{34}/\Phi_{32}) \quad (7)$$

$P_{o,32}/P_{o,34}$ ranged between 1.067 and 1.083, highly correlated with diode laser temperature. Using modeled line strengths, σ_{32}/σ_{34} was estimated to be $(6.25 \pm 0.86) \times 10^{-2}$ at 296 K. Temperature fluctuations will affect σ_x by changing the relative ground-state populations of the rovibrational transitions. For ratio measurements, the effect on δ-values was analyzed using $\Delta\delta/\Delta T \approx 1000\Delta E/(k_B T^2)$,[32] where k_B is Boltzmann's constant, ΔE is the ground-state energy difference between the two transitions, and $\Delta\delta^{34}S/\Delta T$ is estimated to be −9‰ K^{-1}. Temperature fluctuations of ±0.35 K were measured, which would result in fluctuations of ∓3.2‰. However, since temperature fluctuations of the aluminum block were not well correlated with signal fluctuations, measurements were not corrected for temperature changes.

Time-Dependent Behavior. In every experiment, SO_2 decreased after entrainment as shown in Figure 3. The time-dependent behavior of SO_2 was analyzed as a first-order decay, $[SO_2]_t/[SO_2]_o = A\exp(-t/\tau) + B$. Fitted values were $A = 0.20 \pm 0.02$, $B = 0.80 \pm 0.02$, and $\tau = 1540 \pm 200$ s. Average decrease in $[SO_2]$ over 15 min was 9%. After pumping the sample cell empty, SO_2 increased with the pump turned off. This increase was not measured quantitatively and had a rise time of several percent over 5 min.

By analyzing all measurements together, temporal trends in $\delta^{34}S$ are more distinguishable. To compare ratio measurements of differing $\delta^{34}S$, normalized $\delta^{34}S$ values were utilized, defined as

$$\overline{\delta^{34}S_t}\ (‰) = 1000[(^{34}S/^{32}S)_t - \langle^{34}S/^{32}S\rangle]/\langle^{34}S/^{32}S\rangle \quad (8)$$

where $\overline{\delta^{34}S_t}$ and $(^{34}S/^{32}S)_t$ represent values at time t. Equation 8 is similar to eq 1 except that the reference value has been replaced by average value of the sample over the measurement period. The magnitude of fractionation in our system was assessed via a linear fit of $\overline{\delta^{34}S_t}$ versus time, shown in Figure 3. The fit revealed slope $(+2.4 \pm 6.5) \times 10^{-4}$ ‰ s^{-1}, which amounts to a fractionation of $\sim+0.2 \pm 0.6$‰ after 15 min.

Measurements of Isotopic Ratios. Time series of $^{34}S/^{32}S$ measurements are shown in Figure 4 for gas samples produced from three materials spanning the lowest $^{34}S/^{32}S$, material D, to the highest, F. Data are a running 5-s average to better depict measurement drift. An individual measurement was 10 coadded, 50-ms scans, equivalent to 0.5-s duty cycle. Standard deviation of individual measurements, interpreted as short-term precision, was 14‰. As Figure 4 shows, there was longer-term measurement drift on the order of 10 s to several minutes. Standard deviation for binned 5-s measurements of $^{34}S/^{32}S$ ranged from 1.6×10^{-4} (3.6‰, sample E1) to 2.9×10^{-4} (6.6‰, sample D1). Typical standard error during a 15-min measurement was 2.4×10^{-5} (0.55‰). Allan-variance analysis, shown in Supporting Information Figure S-3, indicates $\delta^{34}S$ optimal averaging times between 60 and 100 s.

In order to determine $\delta^{34}S$ for each of the solid samples investigated, a reference value, $(^{34}S/^{32}S)_{L,VCDT}$, was established

(31) Bomse, D. S.; Stanton, A. C.; Silver, J. A. *Appl. Opt.* **1992**, *31*, 718−731.

(32) Bergamaschi, P.; Schupp, M.; Harris, G. W. *Appl. Opt.* **1994**, *33*, 7704−7716.

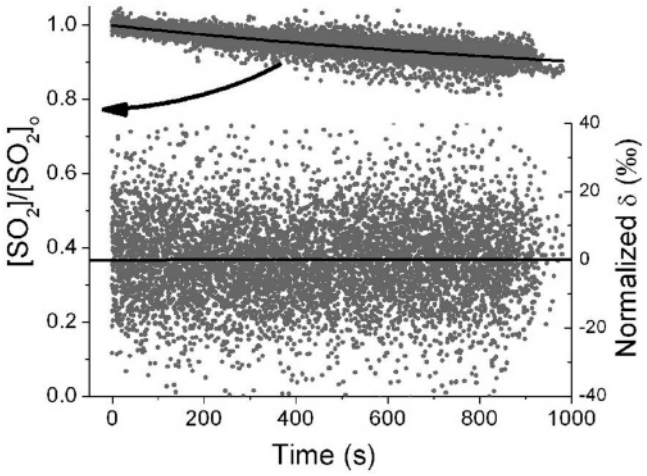

Figure 3. $[SO_2]/[SO_2]_o$ (top) and normalized-$\delta^{34}S$ (bottom) as a function of time. Black line through $[SO_2]/[SO_2]_o$ is a first-order decay fit to the data. Black line through normalized-$\delta^{34}S$ is a linear fit.

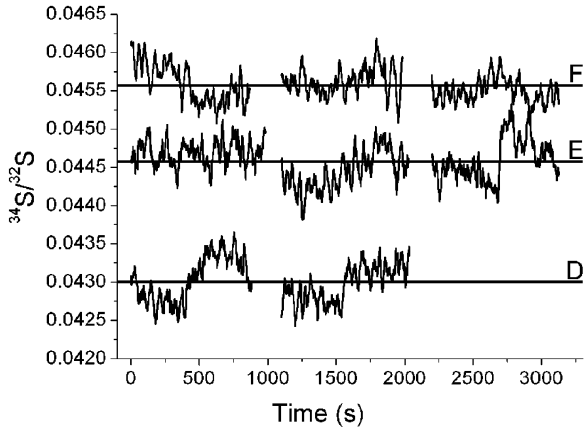

Figure 4. Time series of laser ratio measurements for three different rock types. Data represent 5-s duty cycle average (100 coadded, 50-ms scans). Horizontal lines are the average of all measurements of a particular rock type. Time zero refers to the time at which the first measurement of each rock type occurred.

using measurements of $BaSO_4$ IAEA-SO-5 ($\delta^{34}S = +0.48‰$ VCDT, material E) and extrapolating to 0‰. IAEA-SO-5 was chosen because its $\delta^{34}S$ is close to zero. This reference value was utilized for all reported laser spectroscopic determinations of $\delta^{34}S$. From eq 7, the value of $(^{34}S/^{32}S)_{laser,VCDT}$ was calculated to be 0.044 56, surprisingly close, given the uncertainty in line strengths, to the value determined by Ding et al.[33] of $(^{34}S/^{32}S)_{VCDT} = 0.044\ 164$.

Figure 5 shows laser measurements of $\delta^{34}S$ plotted against mass spectrometer values. A linear fit (dark line) revealed *y*-intercept of 1.5 ± 1.0‰, slope of 1.02 ± 0.05, and correlation coefficient, *R*, of 0.98. The standard deviation between laser and mass spectrometer measured values was 3.7‰. Dashed lines in Figure 5 represent fitted plus and minus one standard deviation. One of the measurements, C1, was well outside this standard deviation. Without this measurement, standard deviation decreased to 2.4‰.

(33) Ding, T.; Valkiers, S.; Kipphardt, H.; De Biévre, P.; Taylor, P. D. P.; Gonfiantini, R.; Krouse, R. *Geochim. Cosomochim. Acta* **2001**, *65*, 2433−2437.

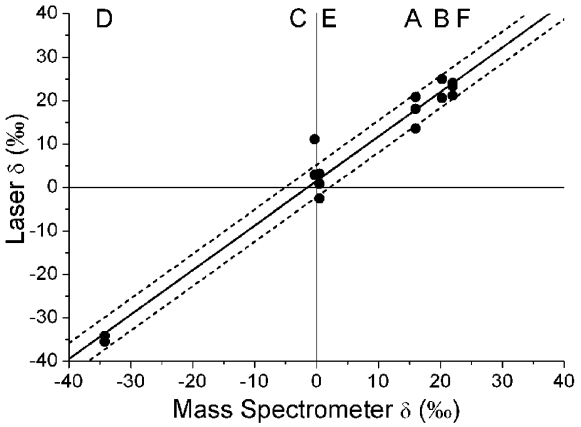

Figure 5. Laser spectrometer versus mass spectrometer $\delta^{34}S$ values. Thick line through the points is a linear fit. The dashed lines to either side represent the standard deviation (1σ) of the laser versus the mass spectrometer measurements. Letters on top are sample designation following from Table 1. All 15 measurements are shown.

DISCUSSION

Possible Fractionation. Decrease in SO_2 after entrainment and its outgassing once the cell was emptied of SO_2, can be explained by invoking a model of reversible sequestration where sulfur dioxide reacts with water on the spectrometer walls via

$$SO_2(g) \rightleftarrows SO_2(aq) \quad (9)$$

$$SO_2(aq) + H_2O \rightleftarrows H^+ + HSO_3^- \quad (10)$$

$$HSO_3^- + H_2O \rightleftarrows H^+ + SO_3^{2-} \quad (11)$$

As SO_2 is assimilated into the water layer, the layer becomes more acidic, which decreases the uptake coefficient of gas-phase SO_2.[34] Sequestration may also occur from SO_2 adsorption on the water surface where SO_2 is bound to the surface by hydrogen bonds though the exact nature of this phenomenon is uncertain.[35] Chemisorption is another sequestration mechanism that may be important.

Sequestration may cause significant fractionation in the remaining gas. Analysis of all normalized $\delta^{34}S$ values indicated fractionation to be +0.2 ± 0.6‰ over 15 min, but interpretation is nontrivial. If SO_2 decay is the result of reactions 9−11, then the system can be interpreted as the establishment of equilibrium between gas-phase SO_2 ($[SO_2]_g$) and sequestered SO_2 ($[SO_2]_{seq}$). From the analysis above, $K_{eq} = k_f/k_r = [SO_2]_{seq,eq}/[SO_2]_{g,eq} = 0.25$, where k_f is the first-order rate coefficient for SO_2 loss to sequestration, k_r is the first-order rate coefficient for SO_2 outgassing from sequestration, and $[SO_2]_{seq,eq}$ and $[SO_2]_{g,eq}$ are their values at equilibrium ($t = \infty$). Integrating the rate equations, $k_r = 1/(1.25\tau) = (5.2 \pm 2.5) \times 10^{-4}\ s^{-1}$, equivalent to a 1/e rise time of ~30 min. Since sequestered SO_2 was not completely removed between experiments, exchange of this remaining SO_2 with a newly entrained gas sample will cause a memory effect. These effects are hidden when averaging many individual runs together. Though

(34) Shimono, A.; Koda, S. *J. Phys. Chem.* **1996**, *100*, 10269−10276.
(35) Tarbuck, T. L.; Richmond, G. L. *J. Am. Chem. Soc.* **2006**, *128*, 3256−3267.

memory effects were not readily apparent in our analysis, they may be revealed with improved measurement accuracy. Regardless of the significance of memory effects, reducing the amount of water that adsorbs onto the walls through specialized coatings[36] is warranted even if only to minimize SO_2(g) loss and maintain a constant environment.

Sources of Noise and Sensitivity Limits. Temperature fluctuations of ±0.35 K, experienced in the present work, are anticipated to affect $\delta^{34}S$ by ∓3.2 ‰ (they are anticorrelated) by changing the relative ground-state populations. Attempts to correlate aluminum block temperature with $\delta^{34}S$ fluctuations from the sample cell proved ineffective. However, better anticorrelation ($R = -0.63$) was observed between aluminum block temperature and reference cell measurements. Peak-to-peak magnitude of reference cell $\delta^{34}S$ fluctuations was nearly twice that of sample cell. The main difference between the cells was the PTFE insert in the sample cell, which separated gas from the aluminum walls with 0.8 cm of PTFE. It may be that this insert insulated the sample cell gas from temperature fluctuations experienced by the aluminum block. To attain measurement sensitivities better than 0.5‰, it is important to measure gas temperature directly, preferably in several locations to discern temperature gradients, and that steps be taken to minimize temperature fluctuations to ±0.1 K or better.

Optical fringe noise is a widely recognized source of noise in laser spectrometers.[37] This noise manifests itself as periodic undulations in acquired spectra with peak-to-peak magnitudes ranging from 10^{-3} or less fractional absorption, highly dependent laser beam alignment, and implementation of fringe-reducing techniques.[38] Mechanical vibration or temperature changes will affect laser beam alignment causing temporal changes in the underlying optical fringe signal. Spectra acquired when no SO_2 was present indicated peak-to-peak amplitudes of optical fringes were observed to be $\sim 2 \times 10^{-4}$ peak-to-peak. Given that fractional absorptions for SO_2 were ~0.15, the peak-to-peak amplitude of noise arising from optical fringes changing with respect to frequency is expected to be ~1.4‰ and may account for some the noise observed in Figure 4. Use of fringe-reducing techniques would significantly reduce this noise.

Standard deviation between laser and mass spectrometer measurements, 3.7‰, is nearly 1 order of magnitude worse than observed by others investigating CO_2 isotope ratios with laser spectroscopy.[8,9] Though SO_2 presents a more complicated problem for isotopic analysis due to its reactivity, direct measurements of gas temperature, minimization of temperature fluctuations, and implementation of fringe-reducing techniques will improve results significantly. More comprehensive study of experimental parameters pressure and fractional absorption is warranted since only a narrow range of pressures (all below 1.6 mbar) and $[SO_2]_o$ (generally within 25% between experiments) were investigated. Of the samples measured at significantly lower pressure and $[SO_2]_o$, C1 and C3, sample C1 had a significantly higher $\delta^{34}S$ value higher than expected, over four standard deviations using the standard deviation of the other measurements (2.4‰).

Outlook. The stated sensitivities were achieved with ~200 nmol total entrained SO_2 in a 14-cm^3 analysis cell with optical path length of 16.5 cm. Orders of magnitude reduction in the amount needed for similar sensitivity should be achieved by utilizing multipass techniques. For instance, the amount of material can be reduced 10-fold by utilizing a commercially available 3600-cm optical path length multipass spectrometer with internal volume of 300 cm^3 (AMAC-36, Aerodyne Research Inc., Billerica, MA) to achieve the same fractional absorption. Far smaller amounts can be analyzed using high-finesse cavities (optical pathlengths $>10^5$ cm) with even smaller sample cell volumes. At quantities of tens of nanomoles or less, laser ablation sampling can be used to produce SO_2 instead of pyrolysis. This presents an intriguing possibility for developing compact and lightweight in situ laser-ablation/laser-spectrometer flight instruments for Earth and planetary studies.

There is a strong $^{33}SO_2$ transition within the spectral region investigated, shown in Figure 2. This creates the opportunity of measuring $\Delta^{33}S$ simultaneously with $\delta^{34}S$. On Mars, measurements of $\Delta^{33}S$ may be crucial in order to differentiate fractionation processes resulting from atmospheric photochemistry from those originating from life.[4] From our FT-IR measurements, the $^{33}SO_2$ feature, which does not overlap other isotopomer transitions, belongs to one of the strongest transitions in the *Q*-branch and likely has ground-state energy less than 200 cm^{-1}, meaning that changes in ground-state population due to temperature fluctuations are relatively small. Further work is underway in our laboratory to determine $^{33}SO_2$ spectral parameters. Also, measuring $\delta^{18}O$ would greatly aid in interpreting measurements. Using the Gaussian 98 suite of programs[39] (B3LYP/6-311+G(3df,p), 0.988 75 frequency scaling), the $SO^{18}O$ band origin is calculated to be 1342.6 cm^{-1} (for comparison, the band origin of $^{34}SO_2$ is ~1344 cm^{-1}) making it probable strong *R*-branch transitions of $SO^{18}O$ are in the vicinity of 1351.7 cm^{-1} with signal strengths half that of $^{33}SO_2$.

CONCLUSIONS

These results represent the first published application of laser spectroscopy to SO_2 isotopic analysis. Sample sizes of ~200 nmol of SO_2 were utilized to achieve 3.7‰ measurement accuracy in $\delta^{34}S$ compared with mass spectrometer measurements. We anticipate achieving sensitivities better than 0.5‰ for $\delta^{34}S$ with further development to reduce temperature and optical fringe noise, similar to development that has occurred for laser spectrometers studying $\delta^{13}C$ in CO_2. The existence of a strong, distinct $^{33}SO_2$ transition with low ground-state energy in the same spectral

(36) Sumner, A. L.; Menke, E. J.; Dubowski, Y.; Newberg, J. T.; Penner, R. M.; Hemminger, J. C.; Wingen, L. M.; Brauers, T.; Finlayson-Pitts, B. J. *Phys. Chem. Chem. Phys.* **2004**, *6*, 604−613.
(37) Werle, P.; Maurer, K.; Kormann, R.; Mucke, R.; D'Amato, F.; Lancia, T.; Popov, A. *Spectrochim. Acta, A* **2002**, *58*, 2361−2372.
(38) Webster, C. R. *J. Opt. Soc. Am., B: Opt. Phys.* **1985**, *2*, 1464−1470.
(39) Frisch, M. J.; Trucks, G. W.; Schlegel, H. B.; Scuseria, G. E.; Robb, M. A.; Cheeseman, J. R.; Zakrzewski, V. G.; Montgomery, J. A., Jr.; Stratmann, R. E.; Burant, J. C.; Dapprich, S.; Millam, J. M.; Daniels, A. D.; Kudin, K. N.; Strain, M. C.; Farkas, O.; Tomasi, J.; Barone, V.; Cossi, M.; Cammi, R.; Mennucci, B.; Pomelli, C.; Adamo, C.; Clifford, S.; Ochterski, J.; Petersson, G. A.; Ayala, P. Y.; Cui, Q.; Morokuma, K.; Malick, D. K.; Rabuck, A. D.; Raghavachari, K.; Foresman, J. B.; Cioslowski, J.; Oritz, J. V.; Baboul, A. G.; Stefanov, B. B.; Liu, G.; Liashenko, A.; Piskorz, P.; Komaromi, I.; Gomperts, R.; Martin, R. L.; Fox, D. J.; Keith, T.; Al-Laham, M. A.; Peng, C. Y.; Nanayakkara, A.; Challacombe, M.; Gill, P. M. W.; Johnson, B.; Chen, W.; Wong, M. W.; Andres, J. L.; Gonzalez, C.; Head-Gordon, M.; Replogle, E. S.; Pople, J. A. *Gaussian 98, Rev. A.9*; Pittsburgh, PA, 2000.

region utilized here for $\delta^{34}S$ will enable simultaneous $\delta^{34}S$ and $\Delta^{33}S$ measurements.

ACKNOWLEDGMENT

This research was carried out by the Jet Propulsion Laboratory (JPL), California Institute of Technology, under contract with the National Aeronautics and Space Administration (NASA) with support from JPL's Research and Technology Development Program via a grant to M.C. and Co-Is. We thank Geoffrey Toon and Jean-François Blavier of JPL for FT-IR analysis of $^{32}SO_2$, $^{33}SO_2$, and $^{34}SO_2$ and Brian Drouin of JPL for the $^{32}SO_2$ sample.

NOTE ADDED AFTER ASAP PUBLICATION

This paper was posted on the Web on 11/17/07. A minor error in the Figure 1 caption was corrected. The paper was reposted on 11/19/07.

SUPPORTING INFORMATION AVAILABLE

Additional information as noted in text. This material is available free of charge via the Internet at http://pubs.acs.org.

Received for review May 21, 2007. Accepted October 1, 2007.

AC071040P